Polymer Chemistry

PAPER

View Article Online
View Journal | View Issue

Cite this: *Polym. Chem.*, 2014, **5**, 6472

Synthesis and morphological studies of a poly(5,6-difluorobenzo-2,1,3-thiadiazole-4,7-diyl-*alt*-quaterchalcogenophene) copolymer with 7.3% polymer solar cell efficiency†

Jhong-Sian Wu, Jyun-Fong Jheng, Jen-Yun Chang, Yu-Ying Lai, Kuan-Yi Wu, Chien-Lung Wang* and Chain-Shu Hsu*

Received 4th June 2014,
Accepted 19th July 2014

DOI: 10.1039/c4py00777h

www.rsc.org/polymers

To obtain a poly(5,6-difluorobenzo-2,1,3-thiadiazole-4,7-diyl-*alt*-quaterchalcogenophene) (**P(FBT-*alt*-CP$_4$)**) copolymer with a small optical band gap (E_g), and to achieve high short-circuit current (J_{sc}) in the **P(FBT-*alt*-CP$_4$)** : $PC_{71}BM$ polymer solar cells (PSCs), **P(FBT-*alt*-Se$_2$Th$_2$)**, which contains selenophene-2,5-diyl (–Se–) π-bridges, was synthesized. **P(FBT-*alt*-Se$_2$Th$_2$)** shows a E_g of 1.56 eV and is strongly aggregated in solution. Wide angle X-ray diffraction (WAXD) and grazing incidence X-ray diffraction (GI-XRD) results revealed the high solid-state order of **P(FBT-*alt*-Se$_2$Th$_2$)** and its edge-on orientation on the substrate. It delivered a high hole mobility (μ_h) of 0.36 $cm^2\ V^{-1}\ s^{-1}$ in organic field-effect transistors (OFETs). The strong aggregation tendency of **P(FBT-*alt*-Se$_2$Th$_2$)** caused large segregation domains in the **P(FBT-*alt*-Se$_2$Th$_2$)** : $PC_{71}BM$ thin film, as is seen in the high-resolution transmission electron microscopy (HR-TEM) images. The addition of 8 vol% of 1-chloronaphthalene (1-CN) effectively suppressed the aggregation and led to more homogeneous active layer morphology. The improved morphology enhanced the J_{sc} of the PSCs. A superior PCE of 7.34% with a V_{oc} of 0.70 V, a J_{sc} of 15.8 mA cm^{-2}, and a FF of 66.4% was achieved in the inverted **P(FBT-*alt*-Se$_2$Th$_2$)** : $PC_{71}BM$ PSCs. The strong aggregation of **P(FBT-*alt*-Se$_2$Th$_2$)** is likely related to its more straight conjugated backbone according to the theoretical calculation results of the **FBT-*alt*-Se$_2$Th$_2$** repeat unit.

Introduction

Conjugated donor–acceptor (D–A) copolymers have been recognized as high-performance materials used in bulk heterojunction (BHJ) polymer solar cells (PSCs).[1] The rapid developments in the molecular design enabled fine tuning of the molecular properties of the D–A copolymers. Along with the morphological optimization of the active layer made of blends of p-type polymers : n-type fullerenes, over 7–8% of power conversion efficiencies (PCEs) in single-junction BHJ PSCs have been realized.[2,3] Moreover, interfacial layer modifications[4] and novel device architectures promoted the PCEs of multiple-junction BHJ PSCs to over 9–10%.[5]

Modulation of the molecular energy levels of the D–A copolymers *via* replacing the chalcogenophene (CP) π-bridges (*i.e.*, furan-2,5-diyl (–Fu–), thiophene-2,5-diyl (–Th–) and selenophene-2,5-diyl (–Se–) groups) have been widely adopted because of the ready availability of the CP units and their significant influences on the molecular properties. In general, copolymers using –Fu– π-bridges have better solubility,[6] lower-lying highest occupied molecular orbital level (E_{HOMO}), and deliver higher open circuit voltage (V_{oc}) than their counterparts.[7] Those employing –Se– π-bridges generally possess more quinoidal character, stabilized E_{LUMO} and narrower E_g.[8,9] Consequently, higher charge mobility (μ) in organic field-effect transistors (OFETs) and short-circuit current (J_{sc}) in BHJ PSCs were delivered by the devices utilizing the –Se– copolymers.[10]

P(FBT-*alt*-Th$_4$) in Scheme 1a is one of the poly(5,6-difluorobenzo-2,1,3-thiadiazole-4,7-diyl-*alt*-quaterchalcogenophene) (**P(FBT-*alt*-CP$_4$)**) copolymers. It has high crystallinity in the solid-state, delivers high hole mobility (μ_h) in organic field-effect transistors (OFETs) and has 6.8% power conversion efficiency (PCE) in BHJ PSCs.[11] However, due to the relatively large E_g of **P(FBT-*alt*-Th$_4$)**, the PCE of the **P(FBT-*alt*-Th$_4$)** : $PC_{71}BM$ PSCs was limited by the low J_{sc}. In attempts to improve the performances of the **P(FBT-*alt*-CP$_4$)**, and to investigate the influences of the –Se– π-bridges on the **P(FBT-*alt*-CP$_4$)** copolymer, in this study, a novel **P(FBT-*alt*-CP$_4$)** copolymer,

Department of Applied Chemistry, National Chiao Tung University, 1001Ta Hsueh Rd., Hsinchu, Taiwan 30010. E-mail: cshsu@mail.nctu.edu.tw, kchwang@nctu.edu.tw

†Electronic supplementary information (ESI) available. See DOI: 10.1039/c4py00777h

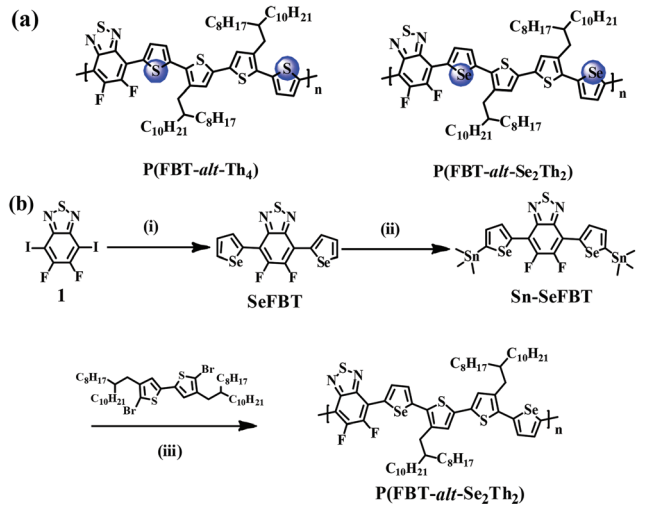

Scheme 1 (a) Chemical structures of **P(FBT-*alt*-Th$_4$)** and **P(FBT-*alt*-Se$_2$Th$_2$)**. (b) Synthetic procedures of **P(FBT-*alt*-Se$_2$Th$_2$)**. Reagents and conditions: (i) 2-(tributylstannyl)selenophene, bis(triphenylphosphine)-palladium(II) dichloride, THF, 70 °C, 12 h; (ii) LDA, dry THF, −78 °C, 1 h; 1 M trimethyltin chloride; (iii) tris(dibenzylideneacetone)dipalladium(0), tri(*o*-tolyl)phosphine, chlorobenzene, 180 °C, microwave 270 W, 50 min.

P(FBT-*alt*-Se$_2$Th$_2$), was synthesized. Replacing the –Th– with the –Se– π-bridges effectively narrows the E_g to 1.56 eV, and results in high J_{sc} of the **P(FBT-*alt*-Se$_2$Th$_2$)** : $PC_{71}BM$ PSCs. The **P(FBT-*alt*-Se$_2$Th$_2$)** : $PC_{71}BM$ PSCs delivered a J_{sc} of 15.8 mA cm^{-2}, and the best PCE of 7.34%. However, the stronger aggregation tendency of **P(FBT-*alt*-Se$_2$Th$_2$)** resulted in large **P(FBT-*alt*-Se$_2$Th$_2$)** segregation domains in the **P(FBT-*alt*-Se$_2$Th$_2$)** : $PC_{71}BM$ active layer, as observed under a high-resolution transmission electron microscope. The process additive, 1-chloronaphthalene, was used to optimize the active layer morphology. The significant changes in the molecular and morphological behaviors caused by the –Se– π-bridges were further scrutinized by morphological analyses and theoretical calculations. It was found that the larger atomic size of selenium improves the backbone linearity, which enhances the aggregation strength and solid-state order of **P(FBT-*alt*-Se$_2$Th$_2$)**.

Experimental section

General measurement and characterization

All chemicals were purchased from Aldrich, Lancaster, TCI or Acros and used as received unless otherwise specified. ^{1}H and ^{13}C NMR spectra were measured using a 400 MHz spectrometer. Differential scanning calorimetry (DSC) was performed on a TA Q200 instrument and thermogravimetric analysis (TGA) was performed on a Perkin Elmer Pyris under a nitrogen atmosphere at a heating rate of 10 °C min^{-1}. Absorption spectra were collected on a HP8453 UV-vis spectrophotometer. The molecular weight of **P(FBT-*alt*-Se$_2$Th$_2$)** was determined with a Viscoteck HTGPC module 350, using trichlorobenzene as the eluent at 140 °C. Electrochemical cyclic voltammetry (CV) was conducted on a CH Instruments Model 611D. A carbon glass electrode coated with a thin polymer film was used as the working electrode and a Ag/Ag^+ electrode was used as the reference electrode, while 0.1 M tetrabutylammonium hexafluorophosphate (Bu_4NPF_6) in acetonitrile was the electrolyte. CV curves were calibrated using ferrocene as the standard, whose oxidation potential was set at −4.8 eV with respect to the zero vacuum level. The E_{HOMO} was deduced from the equation $E_{HOMO} = -e(E_{ox}^{onset} - E_{(ferrocene)}^{onset} + 4.8)$ eV. The E_{LUMO} levels of the polymer were deduced from the equation $E_{LUMO} = -e(E_{red}^{onset} - E_{(ferrocene)}^{onset} + 4.8)$ eV.

X-ray diffractions

The powder X-ray diffraction patterns were recorded at the BL01C2 beamline of the National Synchrotron Radiation Research Center (NSRRC) in Taiwan. The ring energy of NSRRC was operated at 1.5 GeV with a typical current of 300 mA. The wavelength of the incident X-rays was 1.033 Å (12.0 keV), delivered from the superconducting wavelength-shifting magnet, and a Si(111) double-crystal monochromator. The diffraction patterns were recorded at room temperature with a Mar345 imaging plate detector approximately 300 mm from sample positions and a typical exposure duration of 5 minutes. The pixel size of Mar345 was 100 μm. The one-dimensional powder diffraction profile was converted with the program FIT2D and cake-type integration. The diffraction angles were calibrated according to Bragg positions of Ag-behenate and Si powder (NBS640b) standards. The powder sample was sealed in a capillary (1.0 mm diameter); each powder XRD pattern was exposed for about 1.2 minutes. GI XRD measurements were performed at the BL23A end station of the NSRRC, Taiwan. Sample thin films were prepared by spin-casting the copolymer solutions (2.7 mg dissolved in 0.5 mL of ODCB) on Si wafers at 500 rpm. The thin films were then annealed at 200 °C for 1 h. The samples were then placed horizontally on a stage enclosed in an airtight chamber with thin (8 μm) Kapton windows for X-rays. With a 8.0 keV (wavelength λ = 1.550 Å) beam and an incident angle 0.2°, GI XRD was conducted and the pattern was collected with the detector system that included a CMOS flat panel X-ray detector C9728DK (52.8 mm square) situated 7.2 cm from the sample position. The scattering wavevector, defined as $q = 4\pi \sin\theta/\lambda$ (with 2θ being the scattering angle), was calibrated using silver behenate, sodalite, and silicon powders.

Computational details

Quantum-chemical calculations were performed with the Gaussian09 suite employing the WB97XD density functional in combination with the 6-311G(d,p) basis set. Geometry optimizations were performed with tight SCF and convergence criteria and an ultrafine integration grid by applying the GEDIIS optimization algorithm. The minimum nature of each stationary point was confirmed by a frequency analysis.

OFET device fabrication and characterization

An n-type heavily doped Si wafer with a SiO_2 layer of 300 nm and a capacitance of 11 nF cm^{-2} was used as the gate electrode and the dielectric layer. Thin films (40–60 nm in thickness) of polymers were deposited on ODTS treated SiO_2/Si substrates by spin-coating their ODCB solution (5 mg mL^{-1}). The thin films were annealed at 200 °C for 10 minutes. The gold source and drain contacts (40 nm in thickness) were deposited by vacuum evaporation on the organic layer through a shadow mask, affording a bottom-gate, top-contact OFET device. Electrical measurements of the OFET devices were carried out at room temperature in air using 4156C Semiconductor Parameter Analyzers, Agilent Technologies. The field-effect mobility was calculated in the saturation regime by using the equation, $I_{ds} = (\mu WC_i/2L)(V_g - V_t)^2$, where I_{ds} is the drain–source current, μ is the field-effect mobility, W is the channel width (1 mm), L is the channel length (0.1 mm), C_i is the capacitance per unit area of the gate dielectric layer, V_g is the gate voltage and V_t is the threshold voltage.

BHJ PSC fabrication and characterization

The device structures for the conventional PSCs was ITO/PEDOT : PSS/polymer : $PC_{71}BM$/Ca/Al, and ITO/ZnO/polymer : $PC_{71}BM$/MoO_3/Ag for the inverted PSCs. The ITO glass substrates were cleaned with detergent, deionized water, acetone, and isopropyl alcohol in an ultrasonic bath and then dried overnight in an oven at >100 °C. In conventional PSCs, substrates were covered with PEDOT : PSS (40 nm; Al 4083 provided by H. C. Stark) using spin-coating, and dried in a glove box at 150 °C for 30 minutes. Copolymers were dissolved in ODCB, or ODCB containing 8 vol% 1-CN and $PC_{71}BM$ (purchased from Nano-C) was then added into the solution to reach the desired weight ratio. The solution was stirred at 70 °C overnight and filtered through a 0.45 μm filter. In a glove box, the solution of polymer : $PC_{71}BM$ was then spin coated to form the active layer. The cathode made of calcium (35 nm) and aluminum (100 nm) was evaporated through a shadow mask under vacuum (<10^{-6} Torr). For the inverted PSCs, zinc acetylacetonate hydrate (purchased from Aldrich) dissolved in methanol (20 mg mL^{-1}) was spin-casted on pre-cleaned ITO substrates and baked at 130 °C for 10 minutes in the air to form the ZnO layer with a thickness of 30 nm. The active layer was spin-casted on the ZnO layer using the identical procedure mentioned above. The anode made of MoO_3 (6 nm) and Ag (150 nm) was evaporated through a shadow mask under vacuum (<10^{-6} Torr). Each sample consists of four independent pixels defined by an active area of 0.04 cm^2. The devices were characterized in air under 100 mW cm^{-2} AM 1.5 simulated light measurement (Yamashita Denso solar simulator). Current–voltage (J–V) characteristics of PSC devices were obtained by a Keithley2400 SMU. Solar illumination conforming the JIS Class AAA was provided by a SAN-EI 300 W solar simulator equipped with an AM 1.5 G filter. The light intensity was calibrated with a Hamamatsu S1336-5BK silicon photodiode.

Transmission electron microscopy (TEM) observation

TEM observations were performed in bright-field, high-resolution mode on a JEOL JEM-2010 transmission electron microscope with an accelerating voltage of 200 kV equipped with a Gatan-831 CCD camera. The thin-film sample was first spin-coated onto a ITO substrate covered with 40 nm of PEDOT : PSS. The sample was then immersed into water to dissolve the PEDOT : PSS layer and separate the thin films from the ITO substrate. Thin films that floated on the water surface were picked up by copper grids coated with an amorphous carbon layer, dried under vacuum overnight, and used in the TEM observations.

Synthesis of SeFBT

To a round bottom flask were added 5,6-difluoro-4,7-diiodobenzo-2,1,3-thiadiazole **1** (0.5 g, 1.15 mmol), degassed dry THF (50 mL) and $PdCl_2(PPh_3)_2$ (70 mg, 0.104 mmol). The solution was stirred at 70 °C until all the substance completely dissolved. 2-(Tributylstannyl)selenophene (1.33 g, 3.16 mmol) was added dropwise and the mixture was kept at 70 °C for 24 h. After removal of the solvent under reduced pressure, the residue was recrystallized from ethanol to give the product as a red solid. Yield: 450 mg (89%). ^{1}H NMR ($CDCl_3$, 400 MHz): δ (ppm) 8.52 (d, J = 3.6 Hz, 2H), 8.36 (d, J = 2.4 Hz, 2H), 7.52 (t, J = 4.0 Hz, 2H); ^{13}C NMR ($CDCl_3$, 100 MHz): δ (ppm) 110.00, 130.14, 133.00, 133.05, 133.11, 135.37; MS (EI, $C_{14}H_6F_2N_2Se_2S$): calcd, 430.19; found, 430.

Synthesis of Sn-SeFBT

To a solution of compound **SeFBT** (300 mg, 0.70 mmol) in dry THF (50 mL) was added a 2 M solution of lithium diisopropylamide in THF (0.87 mL, 1.74 mmol) dropwise at −78 °C. After stirring at −78 °C for 1 h, 1.0 M solution of chlorotrimethylstannane in THF (2.79 mL, 2.79 mmol) was introduced by a syringe to the solution. The mixture solution was warmed up to room temperature and stirred for 12 h. After removal of the solvent under reduced pressure, the residue was extracted with diethyl ether (50 mL × 3) and water (50 mL). The solvent was evaporated under reduced pressure and the product as a brown solid was obtained by recrystallization from ethanol. Yield: 300 mg (57%). ^{1}H NMR ($CDCl_3$, 400 MHz): δ (ppm) 8.53 (d, J = 4.0 Hz, 2H), 7.68 (d, J = 4.0 Hz, 2H), 0.44 (s, 18 H); MS (EI, $C_{20}H_{22}F_2N_2SSe_2Sn_2$): calcd, 755.80; found, 755.8.

Synthesis of P(FBT-*alt*-Se_2Th_2)

To a 50 mL round bottom flask were added 5,5′-dibromo-4,4′-bis(2-octyldodecyl)-2,2′-bithiophene (113.3 mg, 0.13 mmol), **Sn-SeFBT** (99.3 mg, 0.13 mmol), tris(dibenzylideneacetone) dipalladium (5.9 mg, 0.0065 mmol), tri(2-methylphenyl)phosphine (15.6 mg, 0.052 mmol) and deoxygenated chlorobenzene (5 mL). The mixture was then degassed by bubbling nitrogen for 10 minutes at room temperature. The round bottom flask was put in the microwave reactor and heated to 180 °C at 270 W for 50 minutes. Then, tributyl(thiophen-2-yl)stannane (10.5 mg, 0.028 mmol) was added to the mixture solution and

reacted for 10 minutes at 270 W. Finally, 2-bromothiophene (20 mg, 0.123 mmol) was added to the mixture solution and reacted for 10 minutes at 270 W. After cooling to room temperature the solution was added dropwise to methanol. The precipitate was collected by filtration and washed by Soxhlet extraction with acetone (24 h), hexane (24 h) and tetrahydrofuran (24 h) sequentially. The residue solid was re-dissolved in hot toluene (150 mL). The Pd–thiol gel (Silicycle Inc. 95.1 mg, 0.11 mmol) was added to the above toluene solution to remove the residual Pd catalyst at 80 °C for 12 h. After filtration of the solution and removal of the solvent under reduced pressure, the polymer solution was added into methanol to re-precipitate. The purified polymer was collected by filtration and dried under vacuum for 1 day to give a black solid. The polymer is soluble in warm chlorinated benzenes, but has poor solubility in tetrahydrofuran and chloroform. Yield: 90 mg (60%).

Results and discussion

Synthesis of monomers and polymers

The synthetic route to **P(FBT-*alt*-Se$_2$Th$_2$)** is depicted in Scheme 1b. A Pd-catalyzed Stille-coupling reaction between 5,6-difluoro-4,7-diiodobenzo-2,1,3-thiadiazole (**1**) and 2-(tributylstannyl)selenophene afforded the formation of 5,6-difluoro-4,7-bis(selenophen-2-yl)benzo-2,1,3-thiadiazole (**SeFBT**) in a 89% yield. Lithiation of the **SeFBT** by lithium diisopropylamide (LDA) followed by reacting with trimethyltin chloride resulted in the formation of 5,6-difluoro-4,7-bis(5-(trimethylstannyl)selenophen-2-yl)benzo-2,1,3-thiadiazole (**Sn-SeFBT**) in 57% yield. **Sn-SeFBT** was then copolymerized with 5,5′-dibromo-4,4′-bis(2-octyldodecyl)-2,2′-bithiophene by Stille-coupling to give **P(FBT-*alt*-Se$_2$Th$_2$)**. The number average molecular weights (M_n) and polydispersity index (PDI) are 14.7 kDa and 1.38, respectively, for **P(FBT-*alt*-Se$_2$Th$_2$)** determined by gel permeation chromatography (GPC) using trichlorobenzene as the eluent at 140 °C.

Optical absorption, frontier orbital levels and thermal behaviors

The absorption spectra for the **P(FBT-*alt*-Se$_2$Th$_2$)** in *o*-dichlorobenzne (ODCB) solution and thin film are shown in Fig. 1. In the solution, the absorption bands with λ_{max}s at 430 nm and at 662 nm are attributed to the localized π–π* transition and the photo-induced intramolecular charge transfer (ICT) band of the copolymer. The optical band-gaps (E_g) deduced from the absorption edges of the thin film spectrum is 1.56 eV. Compared to **P(FBT-*alt*-Th$_4$)**,[11] **P(FBT-*alt*-Se$_2$Th$_2$)** exhibited more bathochromic absorption of the ICT band in solution and in the solid state due to the selenophenes introducing more quinoidal character to conjugated polymer backbones.[8d,9] Deduced from cyclic voltammetry measurements (Fig. S1†), the E_{HOMO} and E_{LUMO} of **P(FBT-*alt*-Se$_2$Th$_2$)** are −5.39 eV and −3.70 eV, respectively. Compared to the E_{HOMO} and E_{LUMO} of **P(FBT-*alt*-Th$_4$)**,[11] the smaller E_g of **P(FBT-*alt*-Se$_2$Th$_2$)** is a result of the elevation of E_{HOMO} as shown in Fig. S1b.† The result is unexpected, because in the previous cases,[8a,d,e] the narrower E_g of the –Se– analogues was a result of the deeper-lying E_{LUMO}s instead of the raised E_{HOMO}s. Thus, it is anticipated that the raised E_{HOMO} of **P(FBT-*alt*-Se$_2$Th$_2$)** will decrease the V_{oc} of the **P(FBT-*alt*-Se$_2$Th$_2$)**:PC$_{71}$BM PSCs.

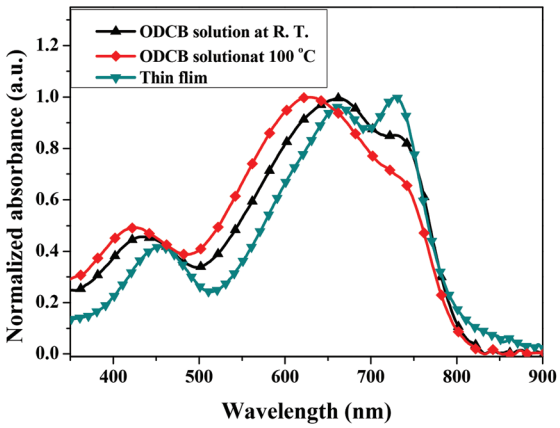

Fig. 1 Normalized solution and thin-film UV-vis absorption spectra of the P(FBT-*alt*-Se$_2$Th$_2$) copolymers.

As shown in Fig. 1, the **P(FBT-*alt*-Se$_2$Th$_2$)** thin film exhibited a strong shoulder band with λ_{max} located at 729 nm. The absorption is an indication of better backbone co-planarity and stronger intermolecular interactions of the conjugated chains in the solid-state.[12] Notably, the shoulder band can also be seen in the ODCB solution, which suggests the aggregation of **P(FBT-*alt*-Se$_2$Th$_2$)** chains in the solution. Rise of solution temperature decreases the degree of aggregation and therefore the absorption intensity of the shoulder band.[13] However, **P(FBT-*alt*-Se$_2$Th$_2$)** maintained 81% of the absorption intensity even at a solution temperature of 100 °C. It is much higher than that of **P(FBT-*alt*-Th$_4$)** (43%) under the same conditions.[11] **P(FBT-*alt*-Se$_2$Th$_2$)** exhibited good thermal stability with decomposition temperature (T_d) at 435 °C determined by thermogravimetric analysis (Fig. S2†). The melting temperatures (T_m) of **P(FBT-*alt*-Se$_2$Th$_2$)** was not found below 350 °C in the differential scanning calorimetry measurement. Because wide angle X-ray diffraction (WAXD) study (*vide infra*) confirms that **P(FBT-*alt*-Se$_2$Th$_2$)** is in its crystalline state at room temperature, the T_m of **P(FBT-*alt*-Se$_2$Th$_2$)** should be above 350 °C, which is higher than the T_m of **P(FBT-*alt*-Th$_4$)** (270 °C). The solution and solid-state behaviors of **P(FBT-*alt*-Se$_2$Th$_2$)** thus suggests that the backbone conformation and the solid-state order of **P(FBT-*alt*-Se$_2$Th$_2$)** are more difficult to be disrupted than its –Th– counterpart.

X-ray structural characterization

Fig. 2a shows the powder WAXD patterns of **P(FBT-*alt*-Se$_2$Th$_2$)**. Three diffraction peaks located at 2θ = 2.91°, 5.82° and 8.73° that possess a scattering factor ratio of 1 : 2 : 3 were observed. It indicates the presence of a long-range ordered lamellar structure with a *d*-spacing of 2.03 nm, and the diffraction peaks can be assigned as the (100), (200) and (300) diffractions

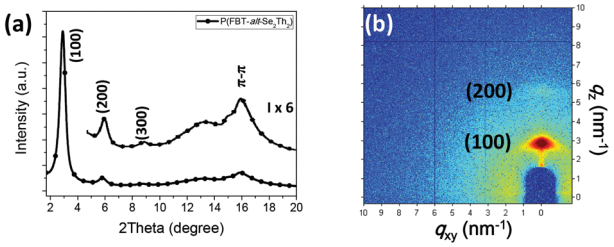

Fig. 2 (a) WAXD pattern and (b) GI-XRD pattern of **P(FBT-*alt*-Se$_2$Th$_2$)**.

for the ordered structure. The diffraction peak located at 2θ = 15.9° (d-spacing of 0.37 nm) represents the ordered π–π stacking of **P(FBT-*alt*-Se$_2$Th$_2$)**. Fig. 2b shows the grazing incidence X-ray diffraction (GI-XRD) pattern of the **P(FBT-*alt*-Se$_2$Th$_2$)** thin film. The (100) and (200) diffraction arcs of the **P(FBT-*alt*-Se$_2$Th$_2$)** lamellar structure were found along the q_z direction, corresponding to the edge-on lamellar stacking of **P(FBT-*alt*-Se$_2$Th$_2$)** on the substrate surface. The XRD results revealed that the solid-state packing of **P(FBT-*alt*-Se$_2$Th$_2$)** is similar to that of **P(FBT-*alt*-Th$_4$)**, which are both featured with long-range ordered lamellar structure and π–π stacking.[11] It also accounts for the more bathochromic shifts of the ICT bands of both **P(FBT-*alt*-Th$_4$)**[11] and **P(FBT-*alt*-Se$_2$Th$_2$)** in the solid state.

OFET and BHJ PSC characteristics

The μ_h of solution-processed **P(FBT-*alt*-Se$_2$Th$_2$)** thin films was measured using a bottom-gate, top-contact device configuration with evaporated gold source/drain electrodes and octadecyltrichlorosilane (ODTS) modified SiO_2 gate dielectric on n-doped silicon wafer surface. The output and transfer plots (at the same source–drain voltages of −80 V) of the devices exhibited typical p-channel OFET characteristics (Fig. 3). The μ_hs were obtained from the transfer characteristics of the devices in the saturation regime. **P(FBT-*alt*-Se$_2$Th$_2$)** exhibited a high μ_h of 0.36 cm^2 V^{-1} s^{-1}with a good on–off ratio of 1.91 × 10^6. Since the solid-state packing of **P(FBT-*alt*-Se$_2$Th$_2$)** and **P(FBT-*alt*-Th$_4$)** is similar, the μ_h of **P(FBT-*alt*-Se$_2$Th$_2$)** is only slightly better than that of **P(FBT-*alt*-Th$_4$)** (μ_h = 0.29 cm^2 V^{-1} s^{-1}).[11]

To evaluate the photovoltaic performances of the copolymers, BHJ PSCs with conventional architecture – ITO/PEDOT : PSS/**P(FBT-*alt*-Se$_2$Th$_2$)** : $PC_{71}BM$ (1 : 1 in wt%)/Ca/Al – and inverted architecture – ITO/ZnO/**P(FBT-*alt*-Se$_2$Th$_2$)** : $PC_{71}BM$ (1 : 1 in wt%)/MoO_3/Ag – were fabricated. Their performances were measured under a simulated AM 1.5 G illumination of 100 mW cm^{-2}. The current density–voltage characteristics of the devices are shown in Fig. 4 and summarized in Table 1. In the conventional architecture, **P(FBT-*alt*-Se$_2$Th$_2$)** : $PC_{71}BM$ PSCs delivered a moderate PCE of 5.47% with a V_{oc} of 0.68 V, a J_{sc} of 12.5 mA cm^{-2}, and a FF of 64.3%. Unexpectedly, the narrower E_g of **P(FBT-*alt*-Se$_2$Th$_2$)** did not promote a higher J_{sc} than those given by the **P(FBT-*alt*-Th$_4$)** : $PC_{71}BM$ PSCs.[11]

To identify the origins of the low J_{sc}, morphological analysis of the **P(FBT-*alt*-Se$_2$Th$_2$)** : $PC_{71}BM$ thin-film was carried out in HR-TEM. As shown in Fig. 5a, deep dark spots were observed in the **P(FBT-*alt*-Se$_2$Th$_2$)** : $PC_{71}BM$ thin film prepared from the

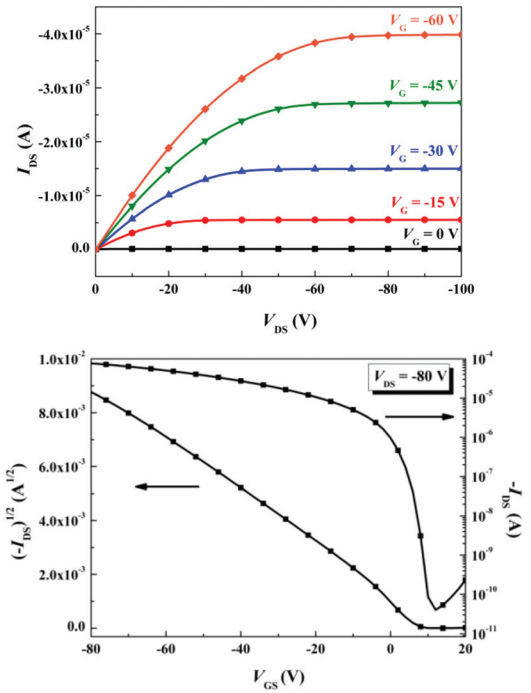

Fig. 3 Typical output curves (up) and transfer plots (down) of the **P(FBT-*alt*-Se$_2$Th$_2$)** OFET devices.

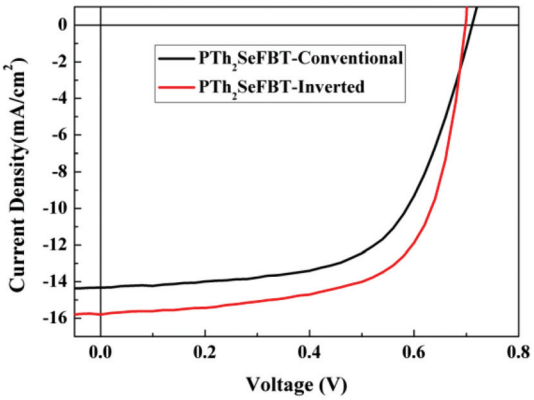

Fig. 4 Current density–voltage characteristics of the **P(FBT-*alt*-Se$_2$Th$_2$)** : $PC_{71}BM$ based BHJ PSCs in the conventional and inverted device architectures under illumination of AM 1.5 G at 100 mW cm^{-2}.

Table 1 PSC characteristics of the **P(FBT-*alt*-Se$_2$Th$_2$)** : $PC_{71}BM$ BHJ PSCs

Architecture	V_{oc} (V)	J_{sc} (mA cm^{-2})	FF (%)	PCE (%)
Conventional	0.68	12.5	64.3	5.47
Conventional[a]	0.72	14.3	61.2	6.31
Inverted[a]	0.70	15.8	66.4	7.34

[a] With 8 vol% of 1-CN as an additive.

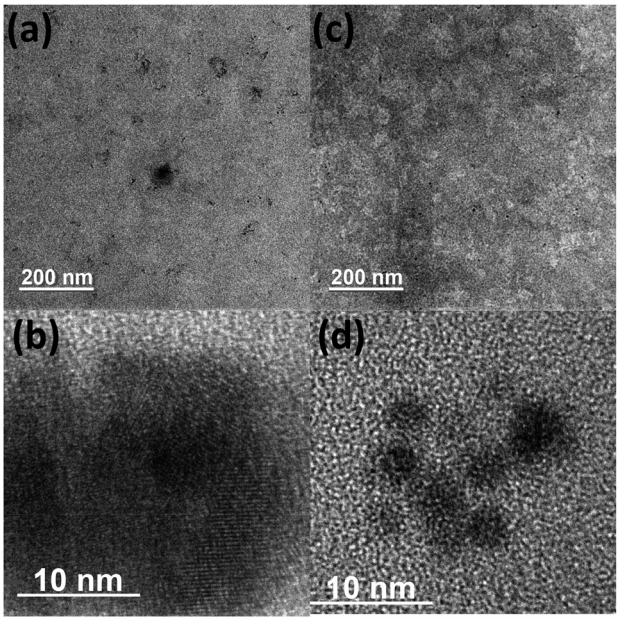

Fig. 5 HR-TEM images of the **P(FBT-*alt*-Se$_2$Th$_2$)** : $PC_{71}BM$ (1 : 1 in wt%) thin films prepared from a ODCB solution at (a) 50k× and (b) 400k× magnifications; **P(FBT-*alt*-Se$_2$Th$_2$)** : $PC_{71}BM$ (1 : 1 in wt%) thin films prepared from a ODCB solution with 8 vol% 1-CN at (c) 50k× and (d) 400k× magnifications.

ODCB solution. The deep dark spots were assigned as the polymer-rich domains, because of the higher atomic scattering factor of the selenium atoms of **P(FBT-*alt*-Se$_2$Th$_2$)**. Fig. 5b shows the image of the dark spot at a higher magnification. Stacks of dark lines, which are separated uniformly with a distance of ~0.37 nm, were observed inside the dark spot. The distance matches the *d*-spacing of the π–π stacking, and further confirmed the dark regions as the polymer-rich domains. The results indicated that **P(FBT-*alt*-Se$_2$Th$_2$)** tends to segregate into large domains in the active layer. To decrease the degree of segregation, 1-CN was used as an additive. With 8 vol% of 1-CN, the population of large dark spots decreased as shown in Fig. 5c. A more homogeneous morphology, which contains interpenetrating polymer-rich (darker regions), and polymer-deficient (brighter regions), was obtained. Although deep dark spots can still be observed in the thin-film (Fig. 5d), their sizes are significantly decreased. Therefore, 1-CN effectively suppressed the segregation of **P(FBT-*alt*-Se$_2$Th$_2$)**, and facilitates the formation of a more homogeneous active morphology.

The morphological changes increased the J_{sc} of the **P(FBT-*alt*-Se$_2$Th$_2$)** : $PC_{71}BM$ PSCs. The PSCs prepared with 8 vol% of 1-CN gave a J_{sc} of 14.3 mA cm^{-2} and a PCE of 6.31%. In inverted PSCs, an even higher PCE of 7.34% with a V_{oc} of 0.70 V, a J_{sc} of 15.8 mA cm^{-2}, and a FF of 66.4% was delivered. Compared to **P(FBT-*alt*-Th$_4$)** : $PC_{71}BM$ PSCs, which delivered a PCE of 6.82% with a V_{oc} of 0.77 V, a J_{sc} of 13.5 mA cm^{-2}, and a FF of 65.6%,[11] the higher-lying E_{HOMO} of **P(FBT-*alt*-Se$_2$Th$_2$)** caused negative impact on the V_{oc}. However, when the morphology of the **P(FBT-*alt*-Se$_2$Th$_2$)** : $PC_{71}BM$ active thin film is optimized, the narrower E_g of **P(FBT-*alt*-Se$_2$Th$_2$)** promoted the J_{sc} and resulted in an overall higher PCE of over 7%.

Theoretical calculations of the P(FBT-*alt*-CP$_4$) copolymers

The molecular properties, solution and solid-state behaviors of **P(FBT-*alt*-Se$_2$Th$_2$)** and **P(FBT-*alt*-Th$_4$)** revealed the remarkable influences of the –CP– π-bridges to the properties of the **P(FBT-*alt*-CP$_4$)** copolymers. The much stronger aggregation tendency of **P(FBT-*alt*-Se$_2$Th$_2$)** significantly affected the solid-state morphology and consequently the performances of the copolymers. Intermolecular non-covalent interactions and molecular geometries are both essential in the aggregation and self-assembly processes.[14] To understand the possible causes of the different aggregation strengths, the dipole moments of the **SeFBT** structural units, and the optimized conformations of the repeat units of **P(FBT-*alt*-Se$_2$Th$_2$)** and **P(FBT-*alt*-Th$_4$)** were further investigated through theoretical calculations.

Fig. S3† shows the optimized structures and the calculated dipole moments of **SeFBT**. The result was obtained *via* theoretical calculations performed with the Gaussian09 suite employing the WB97XD density functional in combination with the 6-311G(d,p) basis set. It was found that the dipole moments of **SeFBT** are comparable to that of 5,6-difluoro-4,7-di(thiophen-2-yl)benzo-2,1,3-thiadiazole (**ThFBT**).[11] Thus, the variation in the π-bridges does not significantly change the dipole moments of the acceptor structural units. In this case, the stronger aggregation tendency of **P(FBT-*alt*-Se$_2$Th$_2$)** cannot be simply attributed to difference in the molecular dipole moment. Fig. 6 shows the optimized conformations of the repeat units of the two **P(FBT-*alt*-CP$_4$)** copolymers. The conformations were obtained through theoretical calculation at the WB97XD/6-311G(d,p) level of density functional theory. The 2-octyldodecyl side chains were replaced by isobutyl groups to keep the branched geometry of the alkyl groups, but avoid excessive computation demand. The calculated bond angles (θ) and bond lengths (L) were summarized in Table 2. θ_1 and θ_2 are the interannular dihedral angles between the CP unit and its neighboring aromatic units. These angles are nearly identical in both repeat units. Therefore, as can be seen from the side view in Fig. 6, the coplanarity of both repeat units in

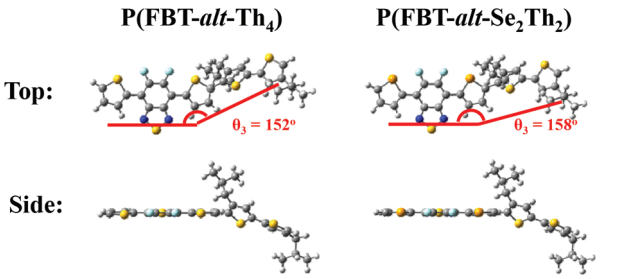

Fig. 6 Top views and side views of the optimized geometries of the repeat units of **P(FBT-*alt*-Th$_4$)** and **P(FBT-*alt*-Se$_2$Th$_2$)** at the WB97XD/6-311G(d,p) level of theory. The atoms are shown in the following colors: sulfur (yellow), selenium (orange), fluorine (light blue), carbon (gray), nitrogen (blue), and hydrogen (light gray).

Table 2 Calculated bond lengths, bond angles, and dihedral angles of the repeat units of the **P(FBT-*alt*-CP$_4$)** copolymers[a]

	X	θ_1 (°)	θ_2 (°)	θ_3 (°)	L_1 (Å)	L_2 (Å)
P(FBT-*alt*-Th$_4$)	S	2.6	−50.2	152	1.75	1.73
P(FBT-*alt*-Se$_2$Th$_2$)	Se	−0.7	−50.7	158	1.89	1.87

[a] Illustration and definition of θ_1, θ_2, θ_3, L_1, and L_2.

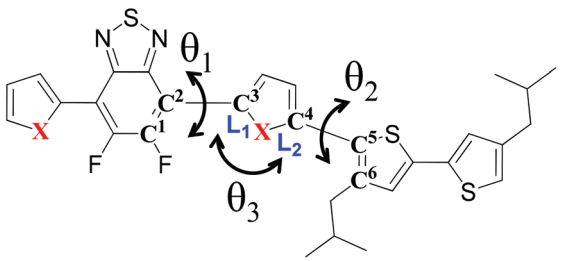

θ_1: dihedral angle of C_1–C_2–C_3–X, θ_2: dihedral angle of X–C_4–C_5–C_6, θ_3: included angle between C_2–C_3 and C_4–C_5 bonds, L_1: bond length of C_3–X bond, L_2: bond length of X–C_4 bond.

their optimized geometries is similar. The main geometrical difference in the repeat units can be found within the –Th– and the –Se– units. Because the van der Waals radius of selenium (1.90 Å) is larger than that of sulfur (1.80 Å),[15] the –Se– unit has longer carbon–heteroatom bonds (L_1 and L_2), and a wider included angle θ_3. Along the chain axis, the wider θ_3 makes the repeat unit of **P(FBT-*alt*-Se$_2$Th$_2$)** less curved than that of **P(FBT-*alt*-Th$_4$)**, as can be seen from the top view of the repeat units in Fig. 6. In summary, the theoretical calculations indicate that the variation in the –CP– π-bridges affects more on the linearity of the repeat units than on the molecular dipole moment and the coplanarity of the repeat units. Thus, it is likely that **P(FBT-*alt*-Se$_2$Th$_2$)** possess stronger aggregation strength because of its more linear backbone geometry. The interannular bond lengths of the repeat units were also and summarized in Table S1.† These lengths are essentially identical in both repeat units.

Conclusions

A novel **P(FBT-*alt*-CP$_4$)** copolymer, **P(FBT-*alt*-Se$_2$Th$_2$)**, was designed and synthesized. Compared to its –Th– analogue, **P(FBT-*alt*-Se$_2$Th$_2$)** possesses a smaller E_g, and an elevated E_{HOMO}. **P(FBT-*alt*-Se$_2$Th$_2$)** strongly aggregates in solution and packed into a long-range ordered lamellar structure and π–π stacking in the solid-state. The T_m of the ordered phase is above 350 °C. Because of its high solid-state order, **P(FBT-*alt*-Se$_2$Th$_2$)** delivered high OFET μ_h of 0.36 cm^2 V^{-1} s^{-1}. When applied to BHJ PSCs, **P(FBT-*alt*-Se$_2$Th$_2$)** segregates into large domains in the **P(FBT-*alt*-Se$_2$Th$_2$)**:PC$_{71}$BM thin film. Addition of 8 vol% of a 1-CN additive prevented strong aggregation of **P(FBT-*alt*-Se$_2$Th$_2$)** and drove the active layer morphology toward ideal bi-continuous interpenetrating network, which consequently promoted the PCE. A superior PCE of 7.34% with a V_{oc} of 0.70 V, a J_{sc} of 15.8 mA cm^{-2}, and a FF of 66.4% was delivered in the inverted **P(FBT-*alt*-Se$_2$Th$_2$)**:PC$_{71}$BM PSC. Theoretical calculations showed that the repeat unit containing the –Se– π-bridges is more linear than the one with the –Th– π-bridges. The strong aggregation strength of **P(FBT-*alt*-Se$_2$Th$_2$)** is thus likely related to its more straight conjugated backbone.

Acknowledgements

This work is supported by the National Science Council and "ATP" of the National Chiao Tung University and Ministry of Education, Taiwan. The authors thank Prof. Keng S. Liang at Institute of Physics, Academia Sinica, Taiwan; Mr Chi-Feng Huang at the Department of Applied Chemistry, National Chiao Tung University; Dr Hwo-Shuenn Sheu at beamline BL01C; Dr U-Ser Jeng and Dr Chun-Jen Su at beamline BL23A of the National Synchrotron Radiation Research Center (NSRRC) in Taiwan for assistance with the XRD measurements.

References

1 M. C. Scharber, D. Wuhlbacher, M. Koppe, P. Denk, C. Waldauf, A. J. Heeger and C. L. Brabec, *Adv. Mater.*, 2006, **18**, 789.

2 (*a*) H. Zhou, L. Yang, A. C. Stuart, S. C. Price, S. Liu and W. You, *Angew. Chem., Int. Ed.*, 2011, **50**, 2995; (*b*) C. M. Amb, S. Chen, K. R. Graham, J. Subbiah, C. E. Small, F. So and J. R. Reynolds, *J. Am. Chem. Soc.*, 2011, **133**, 10062; (*c*) C.-Y. Chang, Y.-J. Cheng, S.-H. Hung, J.-S. Wu, W.-S. Kao, C.-H. Lee and C.-S. Hsu, *Adv. Mater.*, 2012, **2**, 549; (*d*) S. C. Price, A. C. Stuart, L. Yang, H. Zhou and W. You, *J. Am. Chem. Soc.*, 2011, **133**, 4625; (*e*) H. Y. Chen, J. H. Hou, S. Q. Zhang, Y. Y. Liang, G. W. Yang, Y. Yang, L. P. Yu, Y. Wu and G. Li, *Nat. Photonics*, 2009, **3**, 649; (*f*) I. Osaka, T. Kakara, N. Takemura, T. Koganezawa and K. Takimiya, *J. Am. Chem. Soc.*, 2013, **135**, 8834; (*g*) H. Zhong, Z. Li, F. Deledalle, E. C. Fregoso, M. Shahid, Z. Fei, C. B. Nielsen, N. Yaacobi-Gross, S. Rossbauer, T. D. Anthopoulos, J. R. Durrant and M. Heeney, *J. Am. Chem. Soc.*, 2013, **135**, 2040; (*h*) H. J. Son, L. Lu, W. Chen, T. Xu, T. Zheng, B. Carsten, J. Strzalka, S. B. Darling, L. X. Chen and L. Yu, *Adv. Mater.*, 2013, **25**, 838; (*i*) Y.-X. Xu, C. C. Chueh, H.-L. Yip, F.-Z. Ding, Y.-X. Li, C.-Z. Li, X. Li, W.-C. Chen and A. K.-Y. Jen, *Adv. Mater.*, 2012, **24**, 6356; (*j*) J. Cao, Q. Liao, X. Du, J. Chen, Z. Xiao, Q. Zuo and L. Ding, *Energy Environ. Sci.*, 2013, **6**, 3224; (*k*) Y. Li, P. Sonar, L. Murphy and W. Hong, *Energy Environ. Sci.*, 2013, **6**, 1684; (*l*) J. W. Jung, F. Liu, T. P. Russell and W. H. Jo, *Energy Environ. Sci.*, 2013, **6**, 3301; (*m*) Y. Li, *Acc. Chem. Res.*, 2012, **45**, 723; (*n*) L. Huo, S. Zhang, X. Guo, F. Xu, Y. Li and J. Hou, *Angew. Chem., Int. Ed.*, 2011, **50**, 9697.

3 (*a*) H. Xin, X. Guo, G. Ren, M. D. Watson and S. A. Jenekhe, *Adv. Energy Mater.*, 2012, **2**, 575; (*b*) S. Kwon, J. K. Park, G. Kim, J. Kong, G. C. Bazan and K. Lee, *Adv. Energy Mater.*, 2012, **2**, 1420; (*c*) Y. Liang, Z. Xu, J. Xia, S.-T. Tsai, Y. Wu, G. Li, C. Ray and L. Yu, *Adv. Mater.*, 2010, **22**, E135; (*d*) J. T. Rogers, K. Schmidt, M. F. Toney, E. J. Kramer and G. C. Bazan, *Adv. Mater.*, 2011, **23**, 2284; (*e*) J. K. Lee, W. L. Ma, C. J. Brabec, J. Yuen, J. S. Moon, J. Y. Kim, K. Lee, G. C. Bazan and A. J. Heeger, *J. Am. Chem. Soc.*, 2008, **130**, 3619; (*f*) S. J. Lou, J. M. Szarko, T. Xu, L. Yu, T. J. Marks and L. X. Chen, *J. Am. Chem. Soc.*, 2011, **133**, 20661; (*g*) J. S. Moon, C. J. Takacs, S. Cho, R. C. Coffin, H. Kim, G. C. Bazan and A. J. Heeger, *Nano Lett.*, 2010, **10**, 4005; (*h*) J. Peet, J. Y. Kim, N. E. Coates, W. L. Ma, D. Moses, A. J. Heeger and G. C. Bazan, *Nat. Mater.*, 2007, **6**, 497; (*i*) H.-C. Liao, C.-S. Tsao, Y.-T. Shao, S.-Y. Chang, Y.-C. Huang, C.-M. Chuang, T.-H. Lin, C.-Y. Chen, C.-J. Su, U. S. Jeng, Y.-F. Chen and W.-F. Su, *Energy Environ. Sci.*, 2013, **6**, 1938; (*j*) M. Pfannmoller, W. Kowalsky and R. R. Schroder, *Energy Environ. Sci.*, 2013, **6**, 2871.

4 (*a*) Z. He, C. Zhong, X. Huang, W.-Y. Wong, H. Wu, L. Chen, S. Su and Y. Cao, *Adv. Mater.*, 2011, **23**, 4636; (*b*) S.-H. Liao, H.-J. Jhuo, Y.-S. Cheng and S.-A. Chen, *Adv. Mater.*, 2013, **25**, 4766; (*c*) Y.-J. Cheng, C.-H. Hsieh, T. He, C.-S. Hsu and Y. Li, *J. Am. Chem. Soc.*, 2010, **132**, 17381; (*d*) C.-H. Hsieh, Y.-J. Cheng, P.-J. Li, C.-H. Chen, M. Dubosc, R.-M. Liang and C.-S. Hsu, *J. Am. Chem. Soc.*, 2010, **132**, 4887; (*e*) K. M. O'Malley, C.-Z. Li, H.-L. Yip and A. K.-Y. Jen, *Adv. Energy Mater.*, 2012, **2**, 82; (*f*) C.-Y. Chang, L. Zuo, H.-L. Yip, Y. Li, C.-Z. Li, C.-S. Hsu, Y.-J. Cheng, H. Chen and A. K.-Y. Jen, *Adv. Funct. Mater.*, 2013, **23**, 5084.

5 (*a*) J. You, C.-C. Chen, Z. Hong, K. Yoshimura, K. Ohya, R. Xu, S. Ye, J. Gao, G. Li and Y. Yang, *Adv. Mater.*, 2013, **25**, 3973; (*b*) J. You, L. Dou, K. Yoshimura, T. Kato, K. Ohya, T. Moriarty, K. Emery, C.-C. Chen and J. Gao, *Nat. Commun.*, 2013, **4**, 1446; (*c*) O. Adebanjo, P. Maharjan, P. Adhikary, M. Wang, S. Yang and Q. Qiao, *Energy Environ. Sci.*, 2013, **6**, 3150; (*d*) T. Ameri, N. Li and C. J. Brabec, *Energy Environ. Sci.*, 2013, **6**, 2390; (*e*) C.-C. Chen, L. Dou, J. Gao, W.-H. Chang, G. Li and Y. Yang, *Energy Environ. Sci.*, 2013, **6**, 2714.

6 (*a*) C. H. Woo, P. M. Beaujuge, T. W. Holcombe, O. P. Lee and J. M. J. Fréchet, *J. Am. Chem. Soc.*, 2010, **132**, 15547; (*b*) A. T. Yiu, P. M. Beaujuge, O. P. Lee, C. H. Woo, M. F. Toney and J. M. J. Fréchet, *J. Am. Chem. Soc.*, 2012, **134**, 2180; (*c*) B. M. Kobilka, B. J. Hale, M. D. Ewan, A. V. Dubrovskiy, T. L. Nelson, V. Duzhko and M. Jeffries-EL, *Polym. Chem.*, 2013, **4**, 5329.

7 X. Wang, S. Chen, Y. Sun, M. Zhang, Y. Li, X. Li and H. Wang, *Polym. Chem.*, 2011, **2**, 2872.

8 (*a*) M. Heeney, W. Zhang, D. J. Crouch, M. L. Chabinyc, S. Gordeyev, R. Hamilton, S. J. Higgins, I. McCulloch, P. J. Skabara, D. Sparrowe and S. Tierney, *Chem. Commun.*, 2007, 5061; (*b*) S. S. Zade, N. Zamoshchik and M. Bendikov, *Chem. – Eur. J.*, 2009, **15**, 8613; (*c*) Z. Chen, H. Lemke, S. Albert-Seifried, M. Caironi, M. M. Nielsen, M. Heeney, W. Zhang, I. McCulloch and H. Sirringhaus, *Adv. Mater.*, 2010, **22**, 2371; (*d*) B. Kim, H. R. Yeom, M. H. Yun, J. Y. Kim and C. Yang, *Macromolecules*, 2012, **45**, 8658; (*e*) A. A. B. Alghamdi, D. C. Watters, H. Yi, S. Al-Faifi, M. S. Almeataq, D. Coles, J. Kingsley, D. G. Lidzey and A. Iraqi, *J. Mater. Chem. A*, 2013, **1**, 5165.

9 (*a*) H.-Y. Chen, S.-C. Yeh, C.-T. Chen and C.-T. Chen, *J. Mater. Chem.*, 2012, **22**, 21549; (*b*) S. S. Zade, N. Zamoshchik and M. Bendikov, *Chem. – Eur. J.*, 2009, **15**, 8613.

10 (*a*) J. S. Ha, K. H. Kim and D. H. Choi, *J. Am. Chem. Soc.*, 2011, **133**, 10364; (*b*) M. Shahid, T. McCarthy-Ward, J. Labram, S. Rossbauer, E. B. Domingo, S. E. Watkins, N. Stingelin, T. D. Anthopoulos and M. Heeney, *Chem. Sci.*, 2012, **3**, 181; (*c*) J. D. Yuen and F. Wudl, *Energy Environ. Sci.*, 2013, **6**, 392; (*d*) D. H. Wang, A. Pron, M. Leclerc and A. J. Heeger, *Adv. Funct. Mater.*, 2013, **23**, 1297; (*e*) L. Dou, W.-H. Chang, J. Gao, C.-C. Chen, J. You and Y. Yang, *Adv. Mater.*, 2013, **25**, 825; (*f*) M. Shahid, R. S. Ashraf, Z. Huang, A. J. Kronemeijer, T. McCarthy-Ward, I. McCulloch, J. R. Durrant, H. Sirringhaus and M. Heeney, *J. Mater. Chem.*, 2012, **22**, 1281; (*g*) A. J. Kronemeijer, E. Gili, M. Shahid, J. Rivnay, A. Salleo, M. Heeney and H. Sirringhaus, *Adv. Mater.*, 2012, **24**, 1558.

11 J.-F. Jheng, Y.-Y. Lai, J.-S. Wu, Y.-H. Chao, C.-L. Wang and C.-S. Hsu, *Adv. Mater.*, 2013, **25**, 2445.

12 C. Yang, F. P. Orfino and S. Holdcroft, *Macromolecules*, 1996, **29**, 6510.

13 (*a*) B. P. Karsten, L. Viani, J. Gierschner, J. R. M. Cornil and R. A. J. Janssen, *J. Phys. Chem. A*, 2008, **112**, 10764; (*b*) R. Traiphol, N. Charoenthai, T. Srikhirin, T. Kerdcharoen, T. Osotchan and T. Maturos, *Polymer*, 2007, **48**, 813; (*c*) A. P. Zoombelt, M. Fonrodona, M. G. R. Turbiez, M. M. Wienk and R. A. J. Janssen, *J. Mater. Chem.*, 2009, **19**, 5336; (*d*) R. C. Coffin, J. Peet, J. Rogers and G. C. Bazan, *Nat. Chem.*, 2009, **1**, 657; (*e*) R. Steyrleuthner, M. Schubert, I. Howard, B. Klaumünzer, K. Schilling, Z. Chen, P. Saalfrank, F. Laquai, A. Facchetti and D. Neher, *J. Am. Chem. Soc.*, 2012, **134**, 18303.

14 (*a*) S. E. Wheeler, *Acc. Chem. Res.*, 2013, **46**, 1029; (*b*) C. D. Sherrill, *Acc. Chem. Res.*, 2013, **46**, 1020.

15 A. Bondi, *J. Phys. Chem.*, 1964, **68**, 441.